Correlation of hardness and surface microcracking in ITER specification tungsten exposed at QSPA Kh-50

A. Bakaeva [a*], V. Makhlai [b], D. Terentyev [a], A. Zinovev [a, c], S. Herashchenko [b], A. Dubinko [a]

[a] *SCK•CEN, Nuclear Materials Science Institute, Boeretang 200, 2400 Mol, Belgium*

[b] *Laboratory Plasma Accelerators, Institute of Plasma Physics, National Science Center, "Kharkov Institute of Physics and Technology", Akademicheskaya St., 1 61108 Kharkov, Ukraine*

[c] *iMMC, Université catholique de Louvain, Av. Georges Lemaître 4, 1348 Louvain-la-Neuve, Belgium*

Abstract

In this work, we have investigated the evolution of the nanohardness of tungsten under successive thermal shock pulses induced under plasma exposure at quasi-stationary plasma accelerator QSPA-Kh50. The applied conditions represent localized modes of plasma instabilities expected under operation in ITER. The base temperature of 300°C and deposited heat load of 0.45 MJ/m^2 is known to be close to the cracking threshold, which is chosen in this study on purpose. Nanoindentation and microstructural characterization (identification of micro-cracks) is applied to the samples exposed to 10, 50, 70 and 100 pulses to reveal ability of nanoindentation technique to capture the threshold for the micro-crack formation. Knowing that under the selected exposure conditions, the subsurface region of the material is a subject to the recrystallization, which is induced by the overheating during the plasma discharge, nanoindentation measurements are performed on the same tungsten grade annealed at 1300°C, 1500°C and 1800°C to achieve different degree of recrystallization. It is shown that multiple micro-cracks appear after the 50th cycle which correlates with the reduction of the nanohardness corresponding to the massive grain growth. FEM analysis is applied to identify stress/temperature distribution across the sample depth to clarify the nucleation location, expected to occur in the region with the highest stress concentration close to the ductile to brittle transition temperature.

Keywords: tungsten, ITER armor, ELM, thermal shock

***Corresponding author: abakaeva@sckcen.be**

1. Introduction

Due to a number of unique properties, tungsten (W) is selected as the plasma-facing material for the ITER divertor and DEMO first wall [1]. Operation of tungsten in the fusion environment associated with harsh 14 MeV neutron irradiation and cyclic heat loads, induced by plasma instabilities i.e. edge localized modes (ELMs), will inevitably cause modifications in the material microstructure up to the formation of cracks and their propagation through the material [1]. The cracking originates from the penetration of the gaseous atoms inside the material, the formation of bubbles as well as local plastic deformation and grain growth, induced by thermal stresses (see [2] for a recent overview). Testing the material under high heat flux loads, to simulate the critical heat deposition expected under operation of the tokamak, is a part of the qualification program for the approval of the in-vessel

components [3]. The measurements of the residual stresses and non-destructive ultra-sonic inspection on the surface of the tested components is the standard practice for the integrity assessment.

The residual stresses in tungsten after repetitive ITER ELM-like plasma pulses have been measured in recent experiments after the exposure at the quasi-stationary plasma accelerator QSPA Kh-50. The experiments were performed for targets which were preheated at different temperatures (so-called base temperature, T_{base}) varied from room temperature (RT) up to 650°C [4]. The number of exposures was up to 400 pulses with a duration 0.25 ms, and the magnitude of the heat load was below and above the melting threshold. The residual tensile stresses were measured in a thin subsurface layer. The highest stresses (up to 750–850 MPa) were registered after the exposures at T_{base} equal to room temperature and for the energy deposition resulting in the surface temperature to be below the melting threshold. Preheating of the target resulted in the decrease of the residual stresses, as expected due to the dissipation of the stresses by plastic deformation.

Cracking thresholds and crack patterns were studied as well using both plasma accelerators and electron beam [5-11]. Preheated samples of tungsten produced according to the ITER specification (i.e. with elongated grains) were studied at T_{base} around the ductile-to-brittle transition temperature (DBTT), which is in the range of 100-400°C (see summary in ref. [12]). At T_{base} > 300°C, no major cracks are formed on the exposed surfaces, while below DBTT individual cracks and crack networks develop depending on the number of pulses [5]. These results of QSPA plasma exposure were compared with some previous e-beam experiments on thermal shock loads of deformed W material [6]. Similar dimensions of crack meshes were observed in both studies. The observation of micro-crack networks in experiments involving QSPA Kh-50 were attributed to the surface melting and subsequent re-solidification [5]. It was found that by increasing the number of exposures up to 20 plasma pulses of 0.25 ms in duration, the energy threshold for the crack development shifts from 0.3 down to 0.2 MJ/m^2 [13]. A heat load corresponding to the half of the cracking threshold (0.3 MJ/m^2) leads to the appearance of fatigue cracks after 100 plasma pulses. In this case the appearance of cracks could be caused by the accumulation of stress-induced lattice defects (i.e. dislocation lines and forests) which harden the material in the thin plasma-affected sub-surface layer [14]. However, besides the formation of lattice defects, the exposure to heat loads below the melting threshold causes local over-heating of the surface to temperatures exceeding recrystallization limit (1150-1350°C [12]), which induces grain growth and removal of the initial texture. This, in turn, leads to the generation of extended dislocation pile-ups and establishment of stresses near the grain boundaries which eventually causes the crack nucleation. This is why understanding of the dynamics of the recrystallization of the surface prior the crack nucleation is important to envisage and explain thresholds for the crack nucleation.

In this work, we propose an alternative way to study the surface recrystallization due to the plasma exposure by applying nanoindentation testing. Nanoindentation is perfect tool to sense the mechanical response of sub-micrometer volumes and therefore captures tiny changes in the sub-surface microstructure which is not accessible to the conventional hardness measurements. Given the accepted sensitivity of the nanoindentation techniques to the recrystallization, it should be possible to use such measurements for non-destructive analysis. To explore the potential of nanoindentation, we perform plasma exposure using QSPA Kh-50 facilities at base temperature of 300°C, at which the cracking thresholds are well known, for the ITER specification tungsten. The microstructure and "nanohardness" (i.e. hardness measured by nanoindentation) are studied after 10, 50, 70 and 100 cycles to follow the evolution of the damage pattern. To calibrate the response of tungsten in different

microstructural states, nanoindentation is applied to the same tungsten grade annealed at 1300°C, 1500°C and 1800°C. FEM analysis is applied to calculate the distribution of temperature and stress state during and after the exposure cycle depending on the depth, which is then used to discuss the nucleation depth of the cracks under the applied exposure conditions.

2. Experimental details

Polycrystalline W with a purity of 99.97%, provided by Plansee AG as a bar with a square cross-section of 36×36 mm^2 was used in this study and in our previous works, details about impurities and microstructure could be found in [15, 16]. This material was fabricated by hammering on both sides; after the production, the block was stress-relieved at 1000°C for one hour in inert environment. Electron back scattering diffraction (EBSD) analysis revealed that the microstructure of this material consisted of randomly oriented grains, separated mainly by high-angle grain boundaries[17]. Double hammering led to the elongation of grains along the bar axis, as shown on Figure 1 (a). The grain size was found to be about 5-20 µm and 10-100 µm normal and along to the bar axis, respectively.

Figure 1 (b) demonstrates transmission electron microscopy (TEM) image with a typical microstructure of sub-grains present in the material. The sub-grains revealed by TEM are elongated and their size varies in the range 0.6-1.7 µm and 2.3-4.0 µm normal to and along the bar axis direction, respectively [17]. The average dislocation density is about 4.5×10^{12} m^{-2} as was measured in [17].

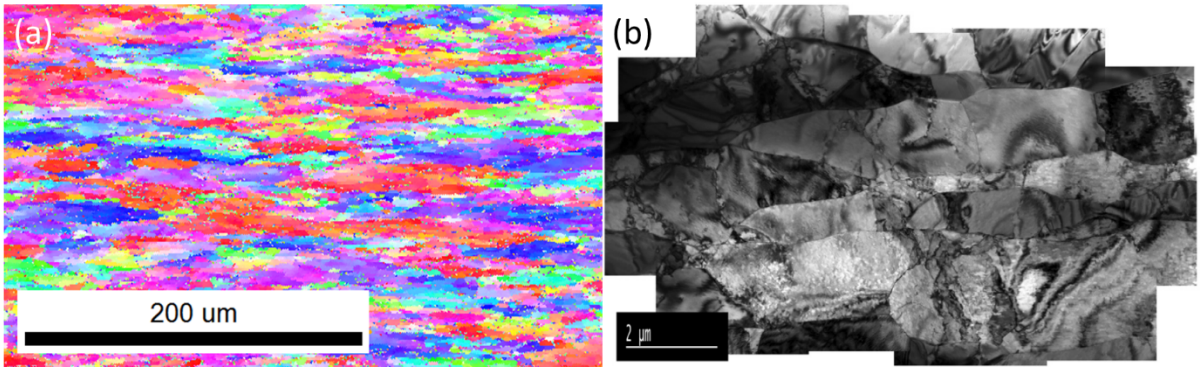

Figure 1 Inverse polar figure map of (a) the EBSD scan and (b) TEM images showing the microstructure of the investigated material.

Prior to any experimental technique was applied, the samples of 10x10x1 mm and 3x10x1 mm (for TEM) were cut and polished. The polishing procedure includes grinding with Struers silicon carbide (SiC) polishing papers (grits of 220, 500, 1200, 2000, 4000 consecutively) and subsequent polishing with a diamond polishing suspension (diamond grain size of 3 µm and 1 µm consecutively).

Exposures to the ELM-like plasma were performed at a quasi-stationary plasma accelerator QSPA Kh-50 in IPP NSC KIPT (Kharkiv, Ukraine) [18]. The main parameters of the hydrogen plasma streams were the following: ion impact energy – about 0.4 keV, maximum plasma pressure – 0.32 MPa, the stream diameter – 18 cm. The plasma pulse shape was approximately triangular and is shown on Figure 2, pulse duration – 0.25 ms. The surface energy load measured with a calorimeter was 0.45 MJ/m^2 (i.e. below tungsten melting threshold being 0.6 MJ/m^2). W targets were preheated to

300°C before plasma pulse with special heater [5]. Temperature was monitored by a calibrated thermocouple.

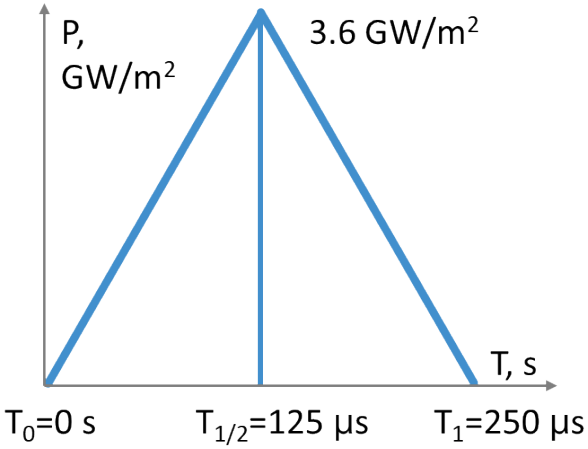

Figure 2. Schematic representation of the plasma pulse shape

After the exposure, the samples were inspected by SEM JEOL JSM-840 to investigate surface roughening and modification and submitted for the nanoindentation measurements. Nanoindentation testing was performed with an Agilent G200 nanoindenter using Continuous Stiffness Mode (CSM) in order to determine the Young's modulus and hardness. The standard XP head equipped with a Berkovich diamond tip was used. The oscillation amplitude and frequency were 2 nm and 45 Hz respectively, the indentation strain rate – 0.05 s^{-1} and the penetration depth *h* – 1.5 μm. At least 25 indents per sample spaced by 40 μm were performed, the hardness was estimated using the classical Oliver & Pharr method [19].

Finite element simulations reproducing the experiment in the QSPA-Kh50 facility were performed with the help of Abaqus. A single heat pulse was simulated at the base temperature 300°C. For simplicity a linear-elastic material was chosen. Its temperature-dependent properties were adopted from the literature: thermal conductivity, specific heat and the coefficient of linear expansion from [20, 21] and the elastic properties from [22]. A block representing a quarter of the tested sample (thus 5x5x1 mm^3) was meshed into 50 000 2nd order hexahedral elements.

The FEM calculations were done in two stages. At the first, purely thermal simulation stage, the evolution of the temperature field was obtained. The top surface was exposed to a 250 μs short heat pulse whose power density evolved in time as shown in Figure 2 so as the absorbed energy density was equal to the experimental value 0.45 MJ/m^2.The bottom face of the block was kept at constant temperature, 300°C. At the second stage, the obtained temporal and spatial distribution of temperature served as input in the mechanical simulations to determine the evolution of stress and strain caused by thermal expansion during and after the heat pulse.

3. Results and Discussion

The results are summarized in three sections reporting the microstructure characterized by SEM, mechanical data obtained by NI techniques and FEM analysis of stress/temperature distributions during and shortly after the pulse.

3.1. Microstructure

The investigation of the material exposed to 10 pulses revealed enhanced surface roughness, see Figure 3 (a and b), but no micro-cracks were observed. The development of both micro- and macro-cracks was observed on the samples exposed to 50 and 70 cycles, see Figure 3 (c-f). The number of macro-cracks increased as the number of pulses raised from 50 to 70. The opening of the macro-cracks reached 3-5 μm, while the walls of the micro-cracks were distant by 0.1-0.2 μm.

After 100 pulses, the macro-cracks were found to be interconnected with each other by micro-cracks thereby forming the network and cells of cracks. Typical cell sizes (see Figure 3) of such crack networks correspond to the grain size and repeat grain pattern. Thus, we consider the observed patterns to be the intergranular cracks (Figure 3 (h)).

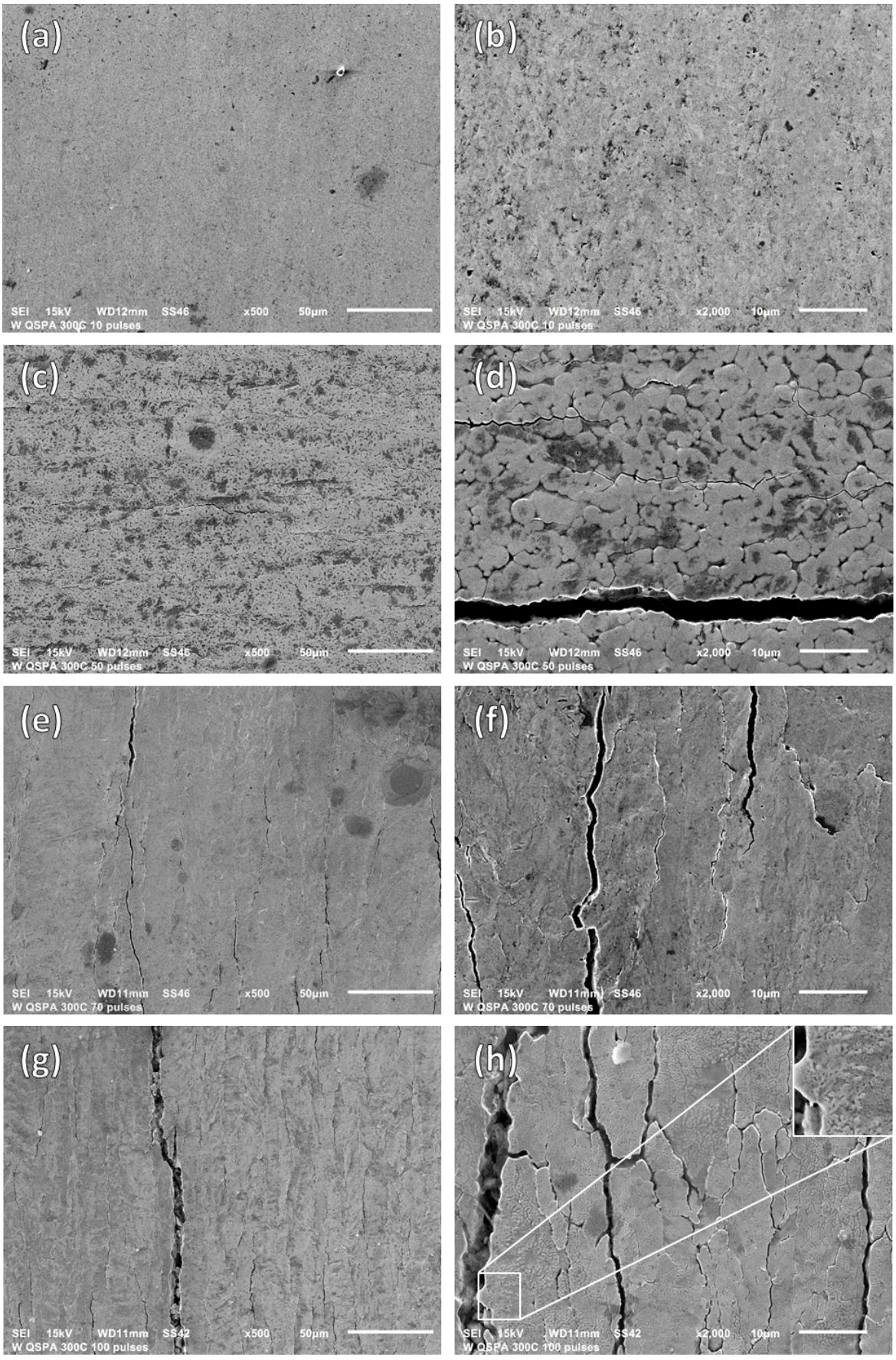

Figure 3 SEM images of W surface after QSPA exposure during (a, e) 10, (c, f) 50, (c, g) 70 and (d, h) 100 pulses.

Similar crack patterns studied in earlier works [5] (the same heat load was applied) were observed at the base temperature of 200°C or lower. The exposures at higher temperature did not yield to the formation cracks, thus implying that the ductile to brittle transition of that W grade was in a range of 200-300°C. The present study suggests that the explored here W grade has a higher transition temperature, being above 300°C. This indeed can be indirectly confirmed by the set of mechanical tests performed recently in [23], which show that the onset of plastic deformation in the transversal orientation occurs above 400°C, while in the longitudinal orientation the material is ductile already at 200°C.

In addition to the observed cracking, the surface melting and re-solidification was observed on the samples exposed to 50 and higher number of the cycles, see Figure 3.

In order to establish the correlation between the microstructure and hardness which was measured on the samples exposed at the QSPA, we performed the annealing of the same material to induce different level of recrystallization. The samples were prepared in the same way as those for the QSPA exposure and then annealed at 1300°C, 1500°C and 1800°C for one hour in vacuum. The resulting EBSD maps are shown in Figure 4. Fig.4(a) represents the material in the stress-relieved state – which was used to perform the QSPA exposures. Annealing at 1300°C causes nucleation of some new grains but the original texture is still preserved as well as strongly elongated grains are still present. After the annealing at 1500°C, the new grains are formed whose shape is equiaxed and the texture is removed. Almost no difference is revealed between the material annealed at 1500°C and 1800°C, which means that 1500°C is enough to induce recrystallization of the initial microstructure on a time scale of an hour or less. TEM analysis was also performed on those samples [24] and it revealed that such annealing caused the decrease of the dislocation density from 4.5×10^{12} m^{-2} down to 6×10^{11} m^{-2} after annealing at 1300°C, to 3×10^{9} m^{-2} at 1500°C and to 1×10^{8} m^{-2} at 1800°C. The latter value was the limit of the TEM resolution. Having these samples well pre-characterized, we move to the results of nanoindentation.

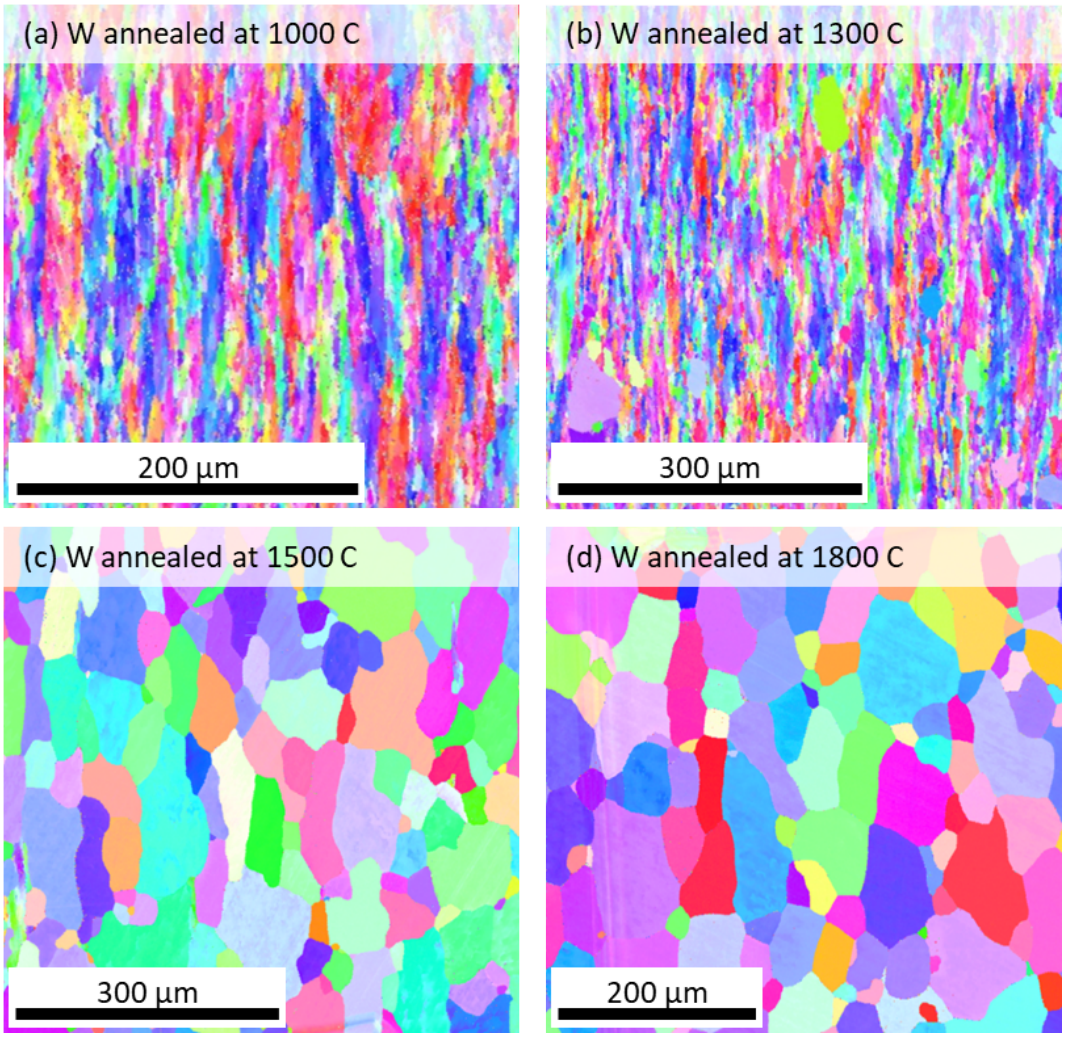

Figure 4 Microstructure of W annealed at (a) 1000°C – corresponding to the stress-relieved state, (b) 1300°C, (c) 1500°C and (d) 1800°C.

3.2. Nanoindentation

The hardness-depth curves calculated from the nanoindentation testing, performed to understand the modification of mechanical properties linked to the change of the microstructure and cracking, are shown in Figure 5. While the maximum indentation depth, *h*, is set as 1.4 µm, the actual response of the material to the penetration of the indenter extends to the region of a factor of 5 larger than *h* [25]. Hence, we are exploring the response of the microstructure within the region of 5-7 µm. As will be shown in Section 3.3, this region is exposed to overheat yielding to the surface temperature of 1900°C and 1800°C at 5 µm depth for the time period of about 125 µs from the moment of the pulse peak.

As is seen from Figure 5 (a), the QSPA exposure results in the reduction of the hardness, compared to the reference material at least within the indentation depth exceeding 0.5 µm. The hardness measured at the indentation depth below 100 nm should be taken with care because of the surface roughness induced by the plasma exposures and therefore we shall not discuss these data and focus on the saturated hardness calculated at the depth of 0.8-1.4 µm. One sees that the saturated

hardness goes does down from 6.4 to 5.4 GPa for the sample exposed to 100 pulses. This reduction is definitely out of the error bar, which is ~0.1 GPa at the depth of 1.4 µm.

Figure 5 (b) presents the hardness-depth curves for the annealed samples. We can see that the annealing also yields to the reduction of the hardness, as expected due to the grain growth (see Figure 4) and removal of the dislocations, which occurs within the whole range of the indentation depth. The annealing at 1500°C results in the strong reduction of the hardness in line with the removal of the elongated grains and formation of new equiaxed grains. No statistically significant difference in the hardness is observed between the samples annealed at 1500°C and 1800°C, which is again consistent with the grain patterns obtained by EBSD for those samples.

Figure 6 demonstrates the saturated hardness H_0, being the hardness at the maximum measured depth of 1500 nm, as a function of annealing temperature. By comparing the saturated hardness of the as-annealed and as-exposed samples, presented in Figure 6, one sees that the softening after the exposure to 10 cycles is equivalent to the annealing at 1300°C, after 50-100 cycles it corresponds to the annealing in the interval of 1300-1500°C, as can be seen from Figure 5 (b). By this comparison, we tend to conclude that the exposure to 10 cycles promotes recovery of the microstructure within the indented region (i.e. within 5-7 µm) but the original texture is preserved. Whereas, the exposure to 50 cycles and a higher number results in the partial recrystallization and judging from the pattern of cracks the grains remain elongated but their size is increased compared to the reference material.

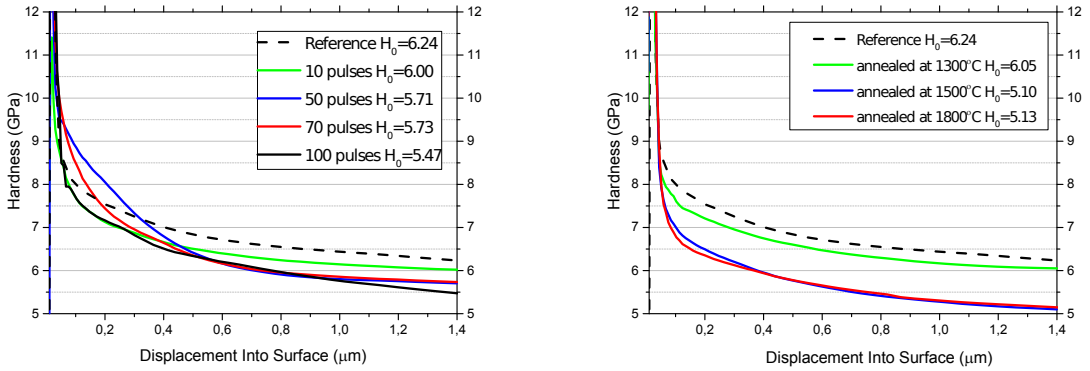

Figure 5 Hardness as functions of the indenter penetration depth, h, for W exposed by (a) QSPA and (b) annealed up to 1800°C.

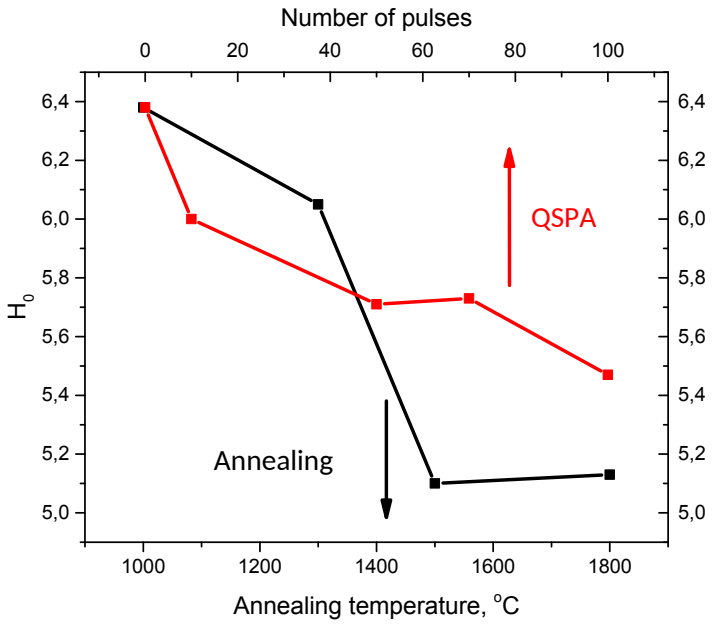

Figure 6 H_0 as a function of annealing temperature and of the number of pulses.

3.3. Temperature/stress distribution

Figure 7 shows the temperature (a and b) and stress (b) in the sample center as a function of depth at the pulse peak, at the temperature maximum and the pulse end, i.e. 125 μs, 175 μs and 250 μs after the beginning of the pulse. The distributions are calculated by FEM set specifically for the geometry of the sample and heat evacuation conditions of the holder implemented at the QSPA for these exposures. The maximum surface temperature is reached after the pulse peak, (at 175 μs), and it amounts to 2200°C. The region heated to the temperature exceeding the recrystallization threshold (around 1300°C) extends up to 50 μm at the pulse peak, and it increases further up to 80 μs at the end

of the pulse (Figure 7 (b)) as a result of the heat conduction. At 50 μs after the end of the pulse, the surface temperature reduces down to 1400°C while the temperature profile at larger depth resembles the one at the end of the pulse. This means that the region heated to the temperature exceeding the recrystallization limit does not spread further than 100 μm and the duration of the overheating period after the pulse is less than 100 μs.

(a) (b)

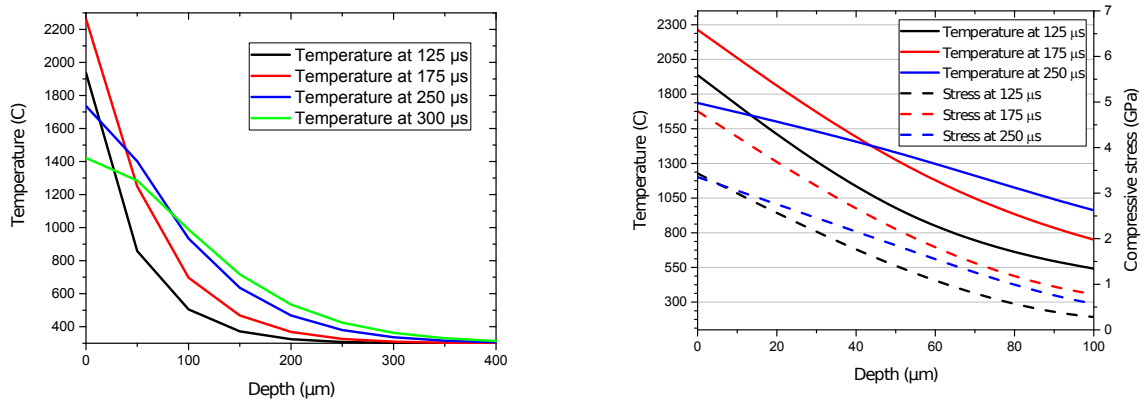

Figure 7 (a) Temperature as a function of depth at 125 μs, 175 μs, 250 μs and 300 μs after the beginning of the pulse. (b) zoom-in of temperature and stress distribution within 100 μs sub-surface layer at 125 μs and 250 μs after the beginning of the pulse.

Figure 7(b) shows the distribution of both temperature and compressive stress in the sub-surface region of 100 μm thickness. The increase of the sub-surface temperature takes place within a period of about 250-300 μs. Intensive recrystallization is expected to occur within first 40 μm from the surface where the temperature exceeds 1500°C. By considering both temperature and stress distribution we see that the compressive stress and temperature monotonically decrease. Keeping in mind that the threshold for the ductile deformation of the studied tungsten in the transversal direction is around 550°C [23], attention should be drawn to the region located at 80-100 μm underneath the surface.

In this region, one can see that at the pulse peak the compressive stress exceeds 500 MPa while the temperature is below 550°C. Given that the ultimate tensile strength for the transversal orientation at 600°C is below 500 MPa [23], the crack nucleation is expected to occur there. Indeed, at a larger depth, the stress level does not exceed the ultimate tensile strength of the material, whereas at smaller depths the material is ductile given rather high local temperature.

(a) Temperature at 125 µs

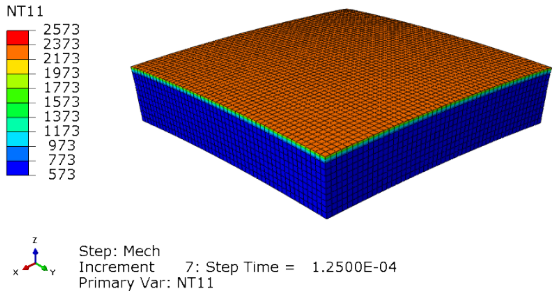

(b) Stress at 125 µs

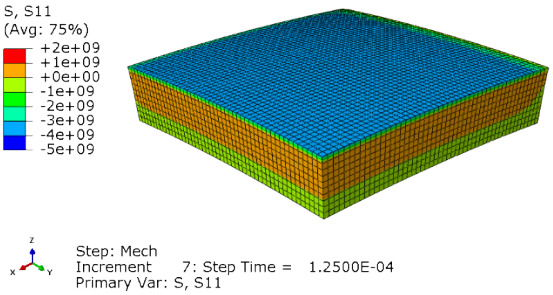

(c) Temperature at 175 µs

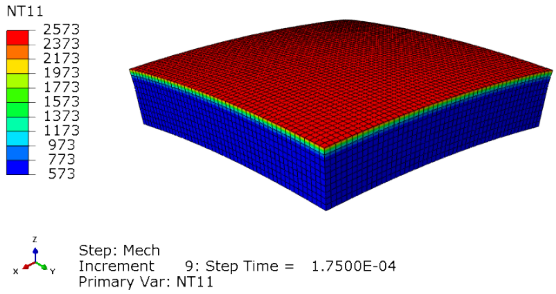

(d) Stress at 175 µs

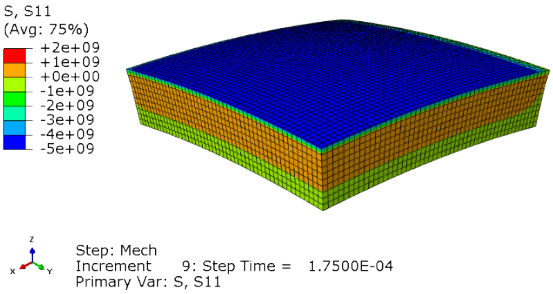

(e) Temperature at 250 µs

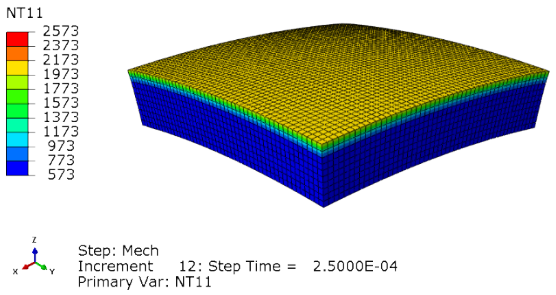

(f) Stress at 250 µs

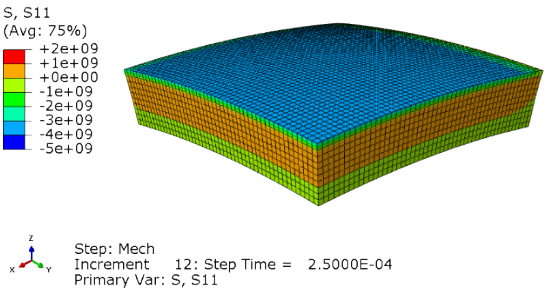

Figure 8 Temperature (K) and stress (Pa) distribution at 125 µs (a, b), 175 µs (c, d), and 250 µs (c, d).

Figure 8 shows the distributions of the normal stress component across the heated surface (S11, measured in Pa) and temperature (NT11, measured in K), recorded at 125 µs, 175 µs and 250 µs, where the sample deformation is magnified by the factor of 10 for clarity. As long as a quarter of the sample was simulated, the visible vertical faces actually represent two perpendicular cross-sections of the sample.

It can be seen that high temperature in the sample exposed to short heat pulses is reached in a thin subsurface region only, however, stress field is much deeper and spreads over the whole sample. The subsurface region experiences high compressive stress, which changes into tensile stress in the middle layer of the sample and changes again into compressive stress at the bottom surface. Hence, in this region the material experiences cyclic deformation which can also cause the nucleation of cracks. Nevertheless, one needs to keep into account the limitations of the currently employed FEM model where purely elastic constitutive law is applied. A thorough investigation of stress concentration and subsequent crack initiation requires the use of elasto-plastic constitutive law valid in a wide range of temperature.

4. Conclusive remarks

We have performed a set of plasma exposures to mimic the thermal shocks due to the edge localized modes expected in the ITER plasma operation. The exposures were performed on the samples made of ITER specification tungsten provided by Plansee AG. The heat load applied in each cycle was 0.45 MJ/m^2 and the base temperature was 300°C which simulates the conditions expected in ITER divertor. The evolution of the surface microstructure was studied by SEM and subsequent modification of the surface hardness was measured by the nanoindentation techniques for the samples exposed to 10, 50, 70 and 100 cycles.

On the basis of the results presented and discussed above, we can summarize the following observations and statements:

- SEM analysis shown that both micro- and macro-cracks were developed on the surface of the samples exposed to 50 and 70 pulses. A number of macro-cracks evidently increases with the number of pulses goes from 50 to 70. After 100 pulses, the macro-cracks are interconnected into the network where the large cracks propagating across the elongated grain boundary interfaces are interconnected by the micro-cracks thereby forming a cell-type structure. A typical dimension of the cells formed by the micro-cracks corresponds to the grain size and crack pattern repeats grain boundary pattern, which is why the cracks are ascribed to be of intergranular type.
- The nanoindentation results show that after the QSPA exposure the hardness goes down i.e. the surface region softens. This reduction of the hardness was compared with the hardness measured in the samples annealed under well controlled conditions to achieve different types of microstructure (in terms of grain size and dislocation density). After 10 cycles, the reduction in the hardening is equivalent to that observed upon the annealing at 1300°C. After 50-70 cycles, the reduction corresponds to the hardness in the range of the values measured for the samples annealed at 1300/1500°C. Hence, the softening measured by the nanoindentation can be attributed to the grain growth caused by overheating during the QSPA pulse.
- FEM analysis has shown that the region heated above 1300°C (i.e. around the recrystallization threshold following the annealing experiments available in literature) extends up to 50 μm in depth in the pulse peak, and extends further up to 80 μs at the end of the pulse. The intensive recrystallization on the time scale of pulse discharge under repetitive pulses is expected to occur within a depth of ~40 μm, where the temperature exceeds 1500°C. The distribution of the compressive stress in the sub-surface shows that it exceeds 1 GPa at the end of the pulse peak within a depth of 80 μm, where the temperature is below 500°C. This region is likely to be the origin of the nucleation of the crack since the compressive stress exceeds the ultimate tensile strength (for the transversal orientation) of the studied material.

Overall, the performed work confirmed earlier results [5-11] regarding the threshold for the crack nucleation, which was obtained for similar tungsten grades using QSPA and electron beam exposure facility. Based on the microstructural analysis, the initiation of cracks was attributed to the recrystallization/grain growth [1], which provokes the formation of long-range pile-ups ahead of grain boundaries and thereby establishes stress concentration. According to such model the nucleation occurs nearby the surface within the first few grains which are subjected to the strong overheating. In this work, we have shown by nanoindentation measurements that there is a good correspondence

between the hardness of the QSPA-exposed samples and hardness of the thermally annealed samples, which achieved the state of recrystallization. In addition, FEM analysis is used to analyze the extension of the sub-surface region where the temperature excursion above recrystallization threshold takes place. The obtained results suggest that the typical depth at which thermo-stress induced crack nucleation occurs is within ~ 40 μm, thus it can be probed by the nanoindentation and micro-indentation techniques as is shown in this work.

Acknowledgements

This work has been carried out within the framework of the EUROfusion Consortium and has received funding from the Euratom research and training program 2014-2018 under grant agreement No 633053. The views and opinions expressed herein do not necessarily reflect those of the European Commission. The author greatly acknowledges help of Marius Wirtz (FZJ) for providing thermally annealed samples for this study.

Data availability

The raw/processed data required to reproduce these findings cannot be shared at this time as the data also forms part of an ongoing study.

References

[1] G. Pintsuk, Tungsten as plasma facing material, Comprehensive Nuclear Materials 4 (2012) 551-581.
[2] O.V. Ogorodnikova, Fundamental aspects of deuterium retention in tungsten at high flux plasma exposure, J Appl Phys 118(7) (2015) 074902.
[3] T. Hirai, S. Panayotis, V. Barabash, Et.al., Use of tungsten material for the ITER divertor, Nuclear Materials and Energy 000 (2016) 1-7.
[4] V.A. Makhlaj, I.E. Garkusha, S.V. Malykhin, A.T. Pugachov, I. Landman, J. Linke, S. Pestchanyi, V.V. Chebotarev, V.I. Tereshin, Residual stresses in tungsten under exposures with ITER ELM-like plasma loads, Phys Scripta T138 (2009) 014060
[5] I.E. Garkusha, I. Landman, J. Linke, V.A. Makhlaj, A.V. Medvedev, S.V. Malykhin, S. Peschanyi, G. Pintsuk, A.T. Pugachev, V.I. Tereshin, Performance of deformed tungsten under ELM-like plasma exposures in QSPA Kh-50, J Nucl Mater 415(1, Supplement) (2011) S65-S69.
[6] T. Hirai, G. Pintsuk, J. Linke, M. Batilliot, Cracking failure study of ITER-reference tungsten grade under single pulse thermal shock loads at elevated temperatures, J Nucl Mater 390-391 (2009) 751-754.
[7] S. Pestchanyi, I. Garkusha, I. Landman, Simulation of residual thermostress in tungsten after repetitive ELM-like heat loads, Fusion Eng Des 86(9) (2011) 1681-1684.
[8] G. Pintsuk, A. Prokhodtseva, I. Uytdenhouwen, Thermal shock characterization of tungsten deformed in two orthogonal directions, J Nucl Mater 417(1) (2011) 481-486.
[9] J. Linke, High Heat Flux Performance of Plasma Facing Materials and Components under Service Conditions in Future Fusion Reactors, Fusion Science and Technology 49(2T) (2006) 455-464.

[10] M. Wirtz, G. Cempura, J. Linke, G. Pintsuk, I. Uytdenhouwen, Thermal shock response of deformed and recrystallised tungsten, Fusion Eng Des 88(9-10) (2013) 1768-1772.
[11] T. Loewenhoff, J. Linke, G. Pintsuk, C. Thomser, Tungsten and CFC degradation under combined high cycle transient and steady state heat loads, Fusion Eng Des 87(7) (2012) 1201-1205.
[12] I. Smid, M. Akiba, G. Vieider, L. Plöchl, Development of tungsten armor and bonding to copper for plasma-interactive components, J Nucl Mater 258-263 (1998) 160-172.
[13] V.A. Makhlaj, I.E. Garkusha, N.N. Aksenov, A.A. Chuvilo, M.S. Ladygina, I. Landman, J. Linke, S.V. Malykhin, S. Pestchanyi, A.T. Pugachev, M.J. Sadowski, E. Skladnik-Sadowska, Simulation of ITER edge-localized modes' impacts on the divertor surfaces within plasma accelerators, Phys Scripta T145 (2011) 014061
[14] V.A. Makhlaj, I.E. Garkusha, N.N. Aksenov, B. Bazylev, I. Landman, J. Linke, S.V. Malykhin, A.T. Pugachov, M.J. Sadowski, E. Skladnik-Sadowska, M. Wirtz, Tungsten damage and melt losses under plasma accelerator exposure with ITER ELM relevant conditions, Phys Scripta T159 (2014) 014024.
[15] A. Dubinko, D. Terentyev, A. Bakaeva, K. Verbeken, M. Wirtz, M. Hernandez-Mayoral, Evolution of plastic deformation in heavily deformed and recrystallized tungsten of ITER specification studied by TEM, Int. Journal of Refractory Metals and Hard Materials 66 (2017) 105-115.
[16] D. Terentyev, G. De Temmerman, T.W. Morgan, Y. Zayachuk, K. Lambrinou, B. Minov, A. Dubinko, K. Bystrov, G. Van Oost, Effect of plastic deformation on deuterium retention and release in tungsten, J Appl Phys 117(8) (2015) 083302.
[17] A. Dubinko, D. Terentyev, A. Bakaeva, K. Verbeken, M.Wirtz, M. Hernández-Mayoral, Evolution of plastic deformation in heavily deformed and recrystallized tungsten of ITER specification studied by TEM, International Journal of Refractory Metals and Hard Materials 66 (2017) 105–115.
[18] I.E. Garkusha, V.A. Makhlai, N.N. Aksenov, B. Bazylev, I. Landman, M. Sadowski, E. Skladnik-Sadowska, Tungsten Melt Losses under QSPA Kh-50 Plasma Exposures Simulating ITER ELMs and Disruptions, Fusion Science and Technology 65(2) (2014) 186-193.
[19] W.C. Oliver, G.M. Pharr, Measurement of hardness and elastic modulus by instrumented indentation: Advances in understanding and refinements to methodology, Journal of Materials Research 19(1) (2004) 3-20
[20] M. Li, E. Werner, J.-H. You, Fracture mechanical analysis of tungsten armor failure of a water-cooled divertor target, Fusion Eng Des 89(11) (2014) 2716-2725.
[21] S.M.J. Janssen, G. Kristo, R. Rouw, J.M.J. Murre, The relation between verbal and visuospatial memory and autobiographical memory, Consciousness and Cognition 31 (2015) 12-23.
[22] R. Lowrie, A.M. Gonas, Single-Crystal Elastic Properties of Tungsten from 24° to 1800°C, J Appl Phys 38 (1967) 4505
[23] C. Yin, D. Terentyev, T. Pardoen, A. Bakaeva, R. Petrov, S. Antusch, M. Rieth, M. Vilémová, J. Matějíček, T. Zhang, Tensile properties of baseline and advanced tungsten grades for fusion applications, International Journal of Refractory Metals and Hard Materials 75 (2018) 153-162.
[24] A. Dubinko, Plastic Deformation of Tungsten under Fusion-Plasma Exposure Conditions, UGent, 2018.
[25] M. Delincé, P.J. Jacques, T. Pardoen, Separation of size-dependent strengthening contributions in fine-grained Dual Phase steels by nanoindentation, Acta Materialia 54(12) (2006) 3395-3404.